Sensitivity Analysis of the Saving Rate Function in the Spatial Solow-Swan Model using PINNs

Gabriel Schmökel[*], **Pedro H. A. Konzen**,
Instituto de Matemática e Estatística, UFRGS,
91509-900, Porto Alegre, RS
E-mail: gabriel.schmokel@ufrgs.br, pedro.konzen@ufrgs.br,

João P. Juchem Neto
Departamento de Economia e Relações Internacionais, UFRGS
90040-000, Porto Alegre, RS
E-mail: plinio.juchem@ufrgs.br.

Abstract: This work investigates the estimation of the savings-rate function in the spatial Solow-Swan model using Physics-Informed Neural Networks (PINNs). Building on previous results in which PINNs successfully recovered the savings-rate function $s(\tilde{x})$ in a controlled case study, we now evaluate the sensitivity of the model's, the observed capital distribution $K(x,t)$ is perturbed by measurement uncertainty. To this end, we introduce homogeneous noise uniformly distributed in $[-\varepsilon,\varepsilon]$ for different levels ε analyze how the estimated $\tilde{s}(x)$ responds to increasing uncertainty. The results show that the estimation remains stable for low to moderate noise levels; however, for higher levels, the errors increase more sharply and the estimated function deteriorates, indicating amplified propagation of uncertainty through the inverse problem. These findings suggest that the PINNs based approach is suitable for noise levels typically associated with empirical Gross Domestic Product (GDP) measurements, supporting its applicability in realistic economic settings.

Palavras-chave: *Inverse Problem, Solow-Swan Spatial Model, PINNs (Physics-Informed Neural Networks), sensitivity Analysis.*

1 Introduction

The classical Solow-Swan model [2, 3] is a central reference in economic growth theory, but its formulation limits the analysis of regional heterogeneity. Spatial extensions [1, 4] overcome this limitation by incorporating diffusion effects and location dependent production. Despite advances in inverse problems within this spatial context [5, 6], we have not identified studies in the literature that estimate a spatially varying savings rate function, leaving this question open.

Physics Informed Neural Networks (PINNs) [7, 8] provide an effective method for inverse problems, especially when data are scarce, by embedding the model equations and their constraints directly into the loss function. In previous, we applied PINNs to estimate the savings rate function $s(x)$ in a case study of the spatial Solow-Swan model. In practice, however, the capital distribution $K(x,t)$ is not directly observed and is often approximated using indicators such as GDP, whose measurement involves uncertainty. Since such are inherently noisy, it becomes essential to assess the sensitivity of the model's estimations of $s(x)$ when the observations used as input are perturbed.

[*]CAPES Master's Scholarship Holder

Motivated by this consideration, the present work investigates how measurement noise in $K(x,t)$ affects the estimation of the function $\tilde{s}(x)$ obtained via PINNs. To this end, we introduce homogeneous noise uniformly distributed in the interval $[-\varepsilon, \varepsilon]$ and test different noise levels to evaluate the sensitivity of the model and identify the levels at which estimation quality begins to deteriorate. The remainder of this work presents the formulation employed, describes the selected and discusses the results obtained for increasing values of ε.

1.1 Model

We consider a model that describes the evolution of capital density in local economies distributed over the compact interval $\Omega = [0, l]$, with $0 < l < \infty$. At each point $x \in \Omega$, there exists a capital density $K(t,x) \geq 0$ and labor density $L(x) \geq 0$, which are used to produce an aggregate good through a Cobb-Douglas production function

$$f(K,L) = A(x)[K^{\phi}(t,x)L^{1-\phi}(x)]. \tag{1}$$

Here, $A(x) > 0$ represents the technological factor and $\phi \in (0,1)$ indicates the intensity of capital in production. The labor distribution is given by the exogenous function $L(x) \geq 0$. Thus, the evolution of the capital stock in the economy is governed by the following reactive-diffusive partial differential equation, with the corresponding initial and boundary conditions

$$K_t = s(x)A(x)\left[K^{\phi}L^{1-\phi}(x)\right] - \delta(x)K + d(x)K_{xx},\ x \in (0,l),\ t > 0, \tag{2a}$$

$$K(t,x) = K_0(x),\ x \in \Omega = [0,l],\ t = 0, \tag{2b}$$

$$K_x = 0,\ x \in \partial\Omega = \{0,l\},\ t > 0. \tag{2c}$$

where $s(x) \in (0,1)$ is the savings rate function we aim to estimate, $\delta(x) \in (0,1)$ is the capital depreciation rate, and $d(x) > 0$ is the capital diffusion coefficient, which represents the intensity of capital movement towards regions with lower available capital. Completing the model, the initial capital distribution, $K_0(x) \geq 0$, is given by Equation (2b), while the homogeneous Neumann boundary conditions, Equation (2c), ensure no transfer of capital and labor at the boundaries $\partial\Omega$, making the economy autarkic.

2 Methodology

2.1 PINNs Method

The inverse problem consists of estimating the savings rate function $s(x)$ from the problem (2) using PINNs with given data $\mathcal{D} = \left\{\left(\hat{t}_i, \hat{x}_i; \hat{K}_i\right)\right\}_{i=1}^{n_d}$, $n_d \geq 1$. The method involves training two neural networks: one to approximate the solution of the PDE problem (2) and another to estimate the savings rate function. Multilayer Perceptron (MLP) networks are employed for this purpose. The first network has inputs (t,x) and outputs the estimated capital density $\tilde{K}(t,x)$, i.e.

$$\tilde{K} = \mathcal{N}_K(t,x;\theta_K), \tag{3}$$

where θ_K denotes the network parameters (weights and biases). The second network has input x and outputs the estimated savings rate function $\tilde{s}(x)$, i.e.

$$\tilde{s}(x) = \mathcal{N}_s(x;\theta_s), \tag{4}$$

with network parameters θ_s.

The network architectures (number of hidden layers and neurons per layer) are chosen based on an exploratory study. The training of both networks is performed simultaneously using the Adam optimizer [9] with a learning rate of 10^{-3} to solve

$$\min_{\theta_K, \theta_s} \mathcal{L}(\theta_K, \theta_s), \tag{5}$$

where $\mathcal{L}(\theta_K, \theta_s)$ is the total loss function defined as

$$\mathcal{L}(\theta_K, \theta_s) = \omega_{PDE}\mathcal{L}_{PDE}(\theta_K, \theta_s) + \omega_{IC}\mathcal{L}_{IC}(\theta_K) + \omega_{BC}\mathcal{L}_{BC}(\theta_K) + \omega_{data}\mathcal{L}_{data}(\theta_K). \tag{6}$$

The first term, $\mathcal{L}_{PDE}(\theta_K, \theta_s)$, represents the loss associated with the residual of the PDE, as follows

$$\begin{aligned}\mathcal{L}_{PDE}(\theta_K, \theta_s) = \frac{1}{n_{PDE}} \sum_{s=1}^{n_{PDE}} \Bigg| &\frac{\partial}{\partial t}\tilde{K}^{(s)}(t_i, x_i; \theta_K) - \tilde{s}(x_i)A(x_i)\left[\tilde{K}^{\phi}(t_i, x_i; \theta_K)L(x_i)^{1-\phi}\right] \\ &+\delta(x_i)\tilde{K}(t_i, x_i; \theta_K) - d(x_i)\frac{\partial^2 \tilde{K}(t_i, x_i; \theta_K)}{\partial x^2}\Bigg|^2,\end{aligned} \tag{7}$$

where n_{PDE} is the number of samples of the PDE. The sample points (t_i, x_i) are randomly selected from the domain $(0, l) \times (0, T)$, with final time $T > 0$. The second and third terms, $\mathcal{L}_{IC}(\theta_K)$ and $\mathcal{L}_{BC}(\theta_K)$ in Equation (6), denote the loss associated with the initial and boundary conditions, respectively. They are the mean squared error of the estimated and expected values of the capital density, derivative on the boundaries of the spatial domain, respectively. The last term, $\mathcal{L}_{data}(\theta_s)$ in Equation (6), represents the loss associated with the observed data points $\mathcal{D}$ for the capital density. It is defined as

$$\mathcal{L}_{data}(\theta_K) = \frac{1}{n_d} \sum_{i=1}^{n_d} \left|\tilde{K}(\hat{t}_i, \hat{x}_i) - \hat{K}_i\right|^2. \tag{8}$$

The weights ω_{PDE}, ω_{IC}, ω_{BC}, and ω_{data} in Equation (6) are hyperparameters that control the penalty of each term in the total loss function. The computations are performed using the PyTorch library in Python.

2.2 Sensitivity Analysis

The sensitivity analysis examines how perturbations in the observed capital data $\mathcal{D}$ affect the reconstructed fields $\tilde{K}(t, x)$ and $\tilde{s}(x)$. Given a noise amplitude $\varepsilon > 0$, we generate perturbed data of the form

$$\hat{K}_i^{(\varepsilon)} = \hat{K}_i + \eta_i, \qquad \eta_i \sim \mathcal{U}(-\varepsilon, \varepsilon), \tag{9}$$

where $\mathcal{U}(-\varepsilon, \varepsilon)$ denotes the uniform distribution on the interval $[-\varepsilon, \varepsilon]$. For each perturbed dataset, the PINN is retrained, producing the reconstructions

$$\tilde{K}^{(\varepsilon)}(t, x), \qquad \tilde{s}^{(\varepsilon)}(x). \tag{10}$$

The error associated with a given noise level is then computed by comparing the noisy reconstruction with the noise-free reference solution:

$$e(\varepsilon) = \|\tilde{s}^{(\varepsilon)} - \tilde{s}^{(0)}\|. \tag{11}$$

3 Results

3.1 Case Study

We begin by proposing a specific case study on n which the sensitivity analysis will later be performed. For this scenario, we aim to obtain the savings rate function by solving the inverse problem given by Equation (2) using PINNs with two MLP networks. This same case study has already been examined by us. More precisely, we consider the setting defined by $l \equiv 10$, $T \equiv 10$, $\phi \equiv 1/3$, $\delta(x) \equiv 0.05$, $A(x) \equiv 1$, $d(x) \equiv 0.25$, and the functions $L(x) = 1 + 0.3, x^2[1 - \cos(4\pi x/l)]$,

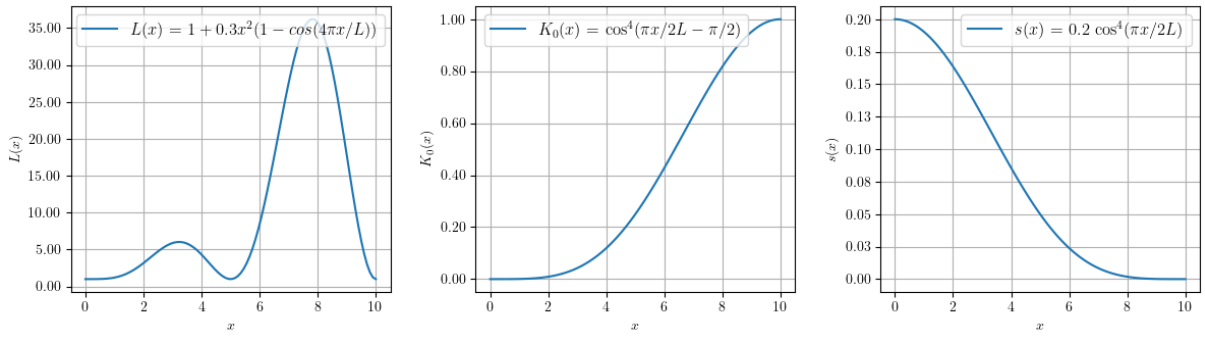

Figure 1: Input functions used in the case study. The labor function $L(x)$, the initial capital distribution $K_0(x)$, and the savings rate function $s(x)$.

$k_0(x) = \cos^4(\pi x/(2l) - \pi/2)$, and $s(x) = 0.2\cos^4(\pi x/(2l))$. These expressions are shown in the Figure 1.

In the adopted PINN methodology, the first network solves the PDE in Equation (2) using (t, x) as inputs, while the second network estimates the savings rate function using only x as input. The training makes use of a dataset of 110 observed points of $K(x, t)$, presented in Figure 2. These values were obtained by solving the forward problem using the Finite Element Method (FEM). All terms of the loss function are equally weighted, with $\omega_{PDE} = \omega_{IC} = \omega_{BC} = \omega_{data} = 1$. The two MLP networks have the architectures $2-n_n^{(K)}\times n_l^{(K)}-1$ and $1-n_n^{(s)}\times n_l^{(s)}-1$,

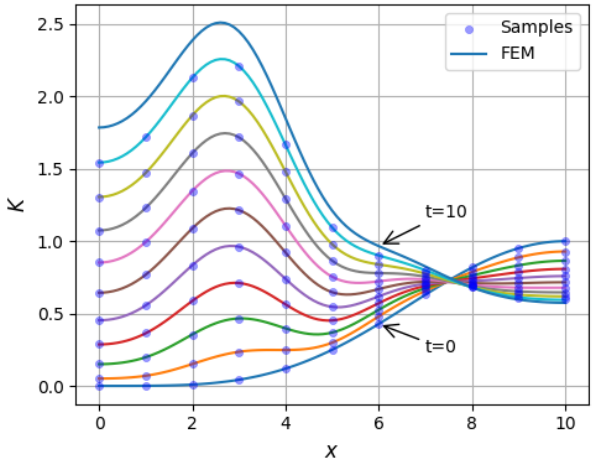

Figure 2: Observed data points for $K(x, t)$ obtained using FEM. Each curve corresponds to a time instant $t \in \{0, 1, \ldots, 10\}$.

where n_n represents the number of neurons per hidden layer, n_l the number of hidden layers in the network, and the upper index identifies the corresponding network: the first network estimates $\tilde{K}(t, x)$, while the second the $\tilde{s}(x)$. To determine the appropriate values of n_n and n_l, we conducted separate studies on the ideal architecture for both approximating the savings rate function $\tilde{s}(x)$ and solving the forward problem defined by Equation (2) using PINNs. Due to the stochastic nature of the procedure (including initialization and the training algorithm), each study was repeated three times. In both cases, we adopted a stopping criterion of $\mathcal{L} < 10^{-5}$, where $\mathcal{L}$ represents the total loss of the MLP in approximating $\tilde{s}(x)$, calculated based on the function provided by the case study, and the total loss in estimating $\tilde{K}(x, t)$, where the capital value $\tilde{K}(x, t)$ was compared with the numerical solution obtained by the finite element method. In all tests performed, the stopping criterion was achievable within 50000 epochs (training iterations).

We concluded that the ideal architectures to solve the inverse problem described by Equation (2) are $2-110\times3-1$ and $1-40\times1-1$, using an input set for the samples with 400. The results obtained with these architectures are shown in Figure 3. The left panel compares the estimated savings rate fSampleunction $\tilde{s}(x)$ with the expected profile, demonstrating close agreement across the entire spatial domain. The right panel displays the reconstructed solution $\tilde{K}(x,t)$ for the time instants $t \in 0,1,\ldots,10$, alongside the corresponding finite element solutions.

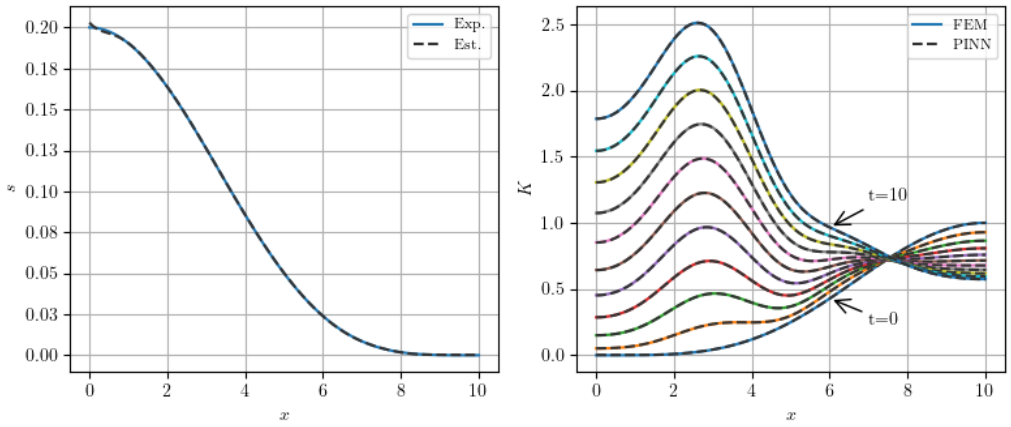

Figure 3: Estimation of the savings rate function $\tilde{s}(x)$ (left) and estimation of $K(x,t)$ over time using PINNs, compared with FEM reference curves (right).

3.2 Sensitivity Analysis

To assess the robustness of the proposed methodology in estimating the savings rate function $\tilde{s}(x)$, we introduced homogeneous noise uniformly distributed in the interval $[-\varepsilon,\varepsilon]$ into the observed data for $K(x,t)$, where ε denotes the noise amplitude. We performed experiments for several noise levels, considering $\varepsilon \in \{0.1\%, 0.5\%, 0.8\%, 1\%, 2\%, 3\%, 5\%, 10\%, 15\%\}$. The preliminary results are summarized in Table 3.2, which reports the estimation errors of $\tilde{s}(x)$ for each noise amplitude using the following metrics: mean squared error (MSE), root mean squared error (RMSE), and relative error (RE).

The results shown in Table 3.2 indicate that, for moderate noise levels, the error metrics do not amplify abruptly, instead, they follow approximately a linear trend with respect to the noise amplitude. This behavior suggests that the methodology maintains stability and a proportional response to data perturbations while ε remains below roughly 10%. However, starting from $\varepsilon = 15\%$, a deviation from this trend becomes apparent: the errors no longer follow the linear growth and begin to increase more sharply. This departure from the near linear regime suggests that higher noise levels start to propagate in an amplified manner through the inverse problem, reducing the accuracy of the estimated function $\tilde{s}(x)$. In summary, the method is robust under low intensity noise, retains predictable behavior for moderate levels, but exhibits loss of stability when the noise reaches higher values.

By fitting a straight line to the relative error values corresponding to noise levels up to $\varepsilon = 10\%$, we observe in the Figure 5 that the resulting linear regression has a slope very close to 1. This reinforces that, in this regime, the relative error grows approximately in the same proportion as the noise amplitude introduced in the data. In practical terms, this proportionality suggests that if the measurement errors in the observed capital data $K(x,t)$ (or, analogously, in empirical GDP data) remain at or below 10%, then the estimated savings rate function $\tilde{s}(x)$ will exhibit an error of comparable magnitude. This behavior reinforces the adequacy of the proposed methodology for applications in which measurement uncertainties are moderate, as the estimation quality remains predictable and directly related to the noise level present in the data.

ε (%)	MSE (10^{-7})	RMSE (10^{-4})	RE (%)
0	2	4	0.3
0.1	6	8	0.7
0.5	9	10	0.9
0.8	13	11	1.1
1	51	22	2.2
2	73	27	2.6
3	140	37	3.6
5	209	46	4.4
10	1466	121	11.5
15	8964	299	28.5

Table 1: Error metrics for the estimated savings rate function $\tilde{s}(x)$ under different noise amplitudes ε.

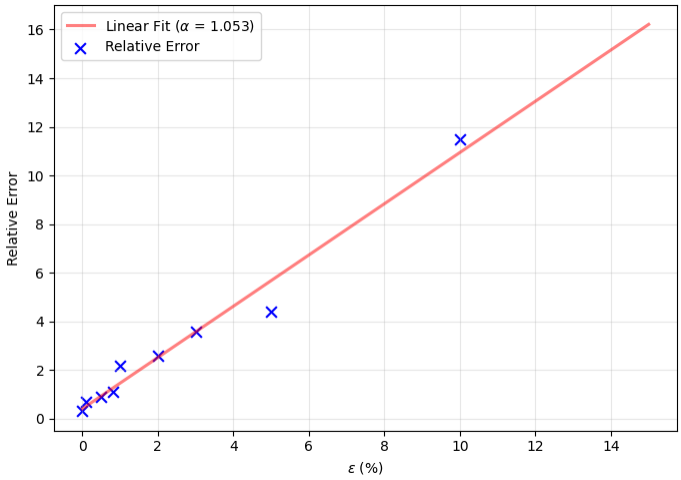

Figure 4: Linear regression of the relative error for noise levels up to $\varepsilon = 10\%$, showing that the error grows approximately proportionally to the noise amplitude.

Figure 5 complements this analysis by illustrating the behavior of the estimated savings rate function $\tilde{s}(x)$ for different values of ε. For low and moderate noise levels ($\varepsilon \leq 1\%$), the reconstructed curves remain close to the expected profile, exhibiting only small localized oscillations. As the noise increases to intermediate values (between 2% and 5%), more noticeable fluctuations appear, although the overall trend of the function is still well captured. For higher noise levels, such as 10% and 15%, the effect of noise becomes more evident, with amplified oscillations and more pronounced deviations from the expected curve. These results are consistent with the previous analysis and reinforce that the methodology remains stable for low to moderate noise levels.

4 Conclusion

The noise analysis shows that the PINN based methodology provides stable and reliable estimates of the savings rate function $\tilde{s}(x)$ under low to moderate levels of measurement uncertainty in $K(x,t)$. For noise amplitudes up to approximately 10%, the error metrics exhibit an almost linear relationship with ε, and the relative error grows proportionally to the introduced perturbation, indicating that the inverse problem remains well behaved in this regime. The estimated savings rate functions also preserve their expected qualitative structure, displaying only small localized oscillations. However, when the noise reaches higher amplitudes, this linear behavior

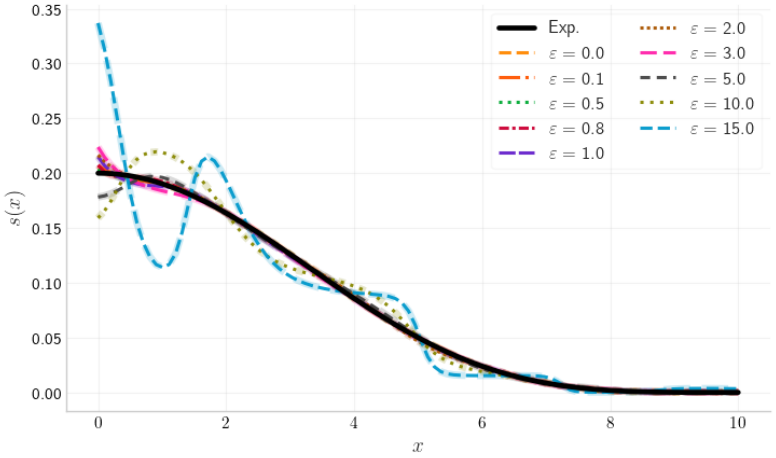

Figure 5: Behavior of the estimated savings-rate function $\tilde{s}(x)$ under increasing noise amplitudes ε.

no longer holds, and both the global error metrics and the shape of $\tilde{s}(x)$ degrade more noticeably, reflecting the amplified propagation of uncertainty through the inverse problem. These results suggest that the method is robust for realistic noise levels typically associated with empirical GDP based measurements.

5 Acknowledgments

The authors thank CAPES for granting the Master's Scholarship, which made this work possible.

References

[1] C. Camacho, B. Zou, "The spatial Solow model", Economics Bulletin, 2004.

[2] T.W. Swan, "Economic Growth and Capital Accumulation", Economic Record, 1956.

[3] R. Solow, "A Contribution to the Theory of Economic Growth", Quarterly Journal of Economics, 70, 65–94, 1956.

[4] J.P. Juchem Neto, J.C.R. Claeyssen, S.S.P Júnior, "Returns to scale in a spatial Solow–Swan economic growth model", Physica A: Statistical Mechanics and its Applications, 2019.

[5] R. Engbers, "Inverse problems in geographical economics: parameter identification in the spatial Solow model", Economic Record, 2014.

[6] W. Hu, "A new method to solve the forward and inverse problems for the spatial Solow model by using Physics Informed Neural Networks (PINNs)", Engineering Analysis with Boundary Elements, 2024.

[7] M. Raissi, P. Perdikaris, G.E. Karniadakis, "Physics-informed neural networks: A deep learning framework for solving forward and inverse problems involving nonlinear partial differential equations", Journal of Computational Physics, 2019.

[8] L. Lu, R. Pestourie, W. Yao, Z. Wang, F. Verdugo, S.G. Johnson, "Physics-Informed Neural Networks with Hard Constraints for Inverse Design", SIAM Journal on Scientific Computing, 2021.

[9] D.P. Kingma e J. Ba, "Adam: A Method for Stochastic Optimization", arXiv:1412.6980, 2017.